Electronic Supplementary Material (ESI) for Environmental Science: Nano.


**Appendix A. Supplementary Data**

# Facile fabrication of Bi nanoparticle-decorated g-$C_3N_4$ photocatalysts for effective tetracycline hydrochloride degradation: environmental factors, degradation mechanism, pathways and biotoxicity evaluation

Dongling Jia,*[a] Yifan Zhang,[a] Xue Zhang,[b] Peiying Feng,[a] Lin Yang,[b] Ruonan Ning,[a] Hongzhi Pan*[a] and Yuqing Miao*[b]

---

[a] *Shanghai University of Medicine & Health Sciences, Shanghai 201318, People's Republic of China*

[b] *University of Shanghai for Science and Technology, Shanghai 200093, People's Republic of China*

** Corresponding authors.*

*E-mail address: jiadongling1@126.com; panhz@sumhs.edu.cn; yqmiao@usst.edu.cn*

**Analysis of TC-H and intermediates**

An ultra-performance liquid chromatograph (UPLC, Waters) equipped with a mass spectrometer (AB Sciex Triple Quad 5500) was used to evaluate the effect of different types of water matrices on low concentration of TC-H during the photocatalytic process. A Waters Acquity BEH C18 column (2.1 mm × 50 mm, 1.7 μm) was employed, and the column temperature was set at 35 °C. The mobile phase was a mixture of 0.1% fomic acid in water (A) and 0.1% fomic acid in MeOH (B) with a flow rate of 0.4 mL $min^{-1}$. The injection volume of samples was 10 μL.

Analysis of photodegradation intermediates was performed by a high-performance liquid chromatograph tandem mass spectrometer (Ultimate 3000 UHPLC-Q Exactive, Thermo Scientific, US) with an Eclipse Plus C18 column (100 mm × 4.6 mm, 5 μm). The mobile phase was 0.1% formic acid solution (A, 80%) and acetonitrile (B, 20%) at flow rate of 0.5 mL $min^{-1}$ with the column temperature of 30 °C. Heated electrospray ionization (HESI) source in positive mode was used to estimate the TC-H and intermediates in the range of 50−600 m/z.

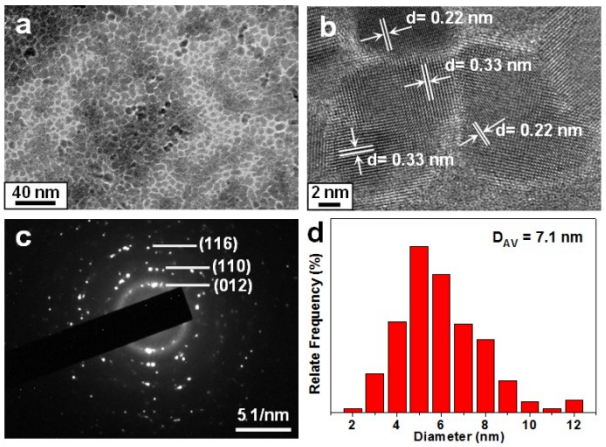


**Fig. S1.** (a) TEM, (b) HR-TEM, (c) SAED pattern and (d) size distribution of the as-prepared Bi nanoparticles.

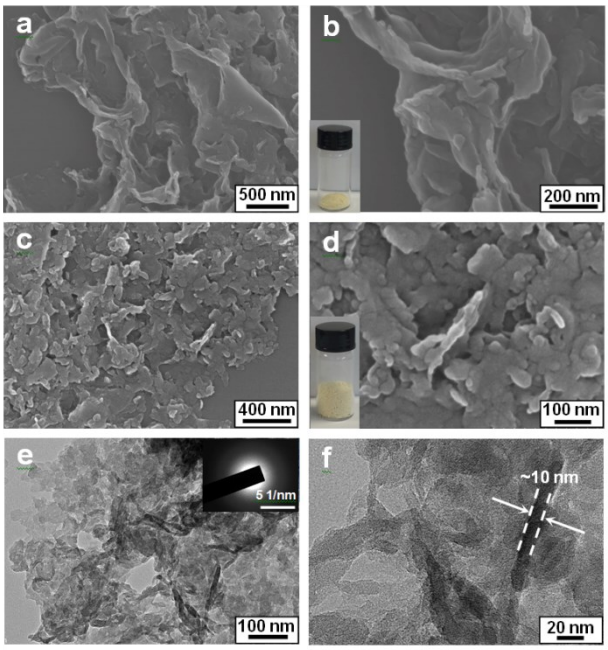


**Fig. S2.** (a,b) SEM images of the bulk g-$C_3N_4$, (c,d) SEM images of the porous g-$C_3N_4$ nanosheets, the insets in (b) and (d) show that the g-$C_3N_4$ nanosheet have a larger volume than bulk g-$C_3N_4$ with the same mass, (e,f) TEM micrographs of g-$C_3N_4$ nanosheets, and the inset in (e) is the SAED pattern of g-$C_3N_4$ nanosheets.

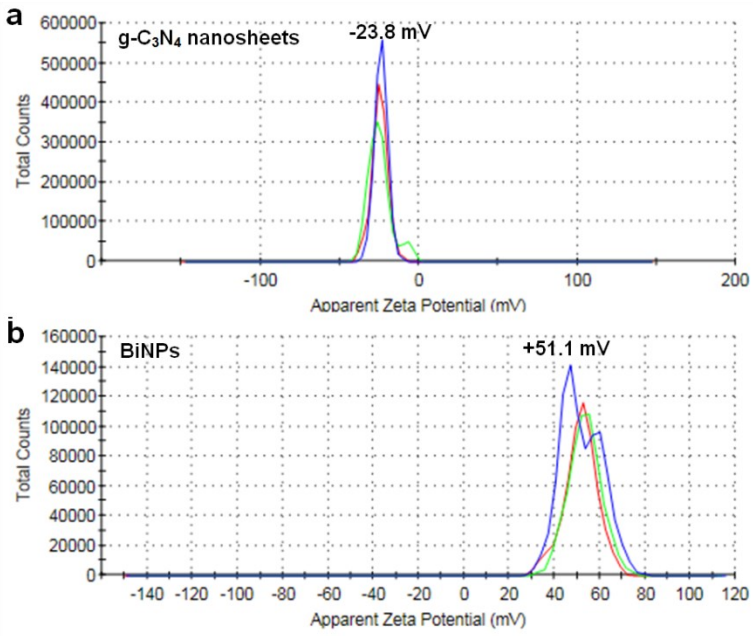


**Fig. S3.** Zeta potential distribution of the exfoliated g-$C_3N_4$ nanosheets (a), and Bi nanoparticles (b) dispersed in water.

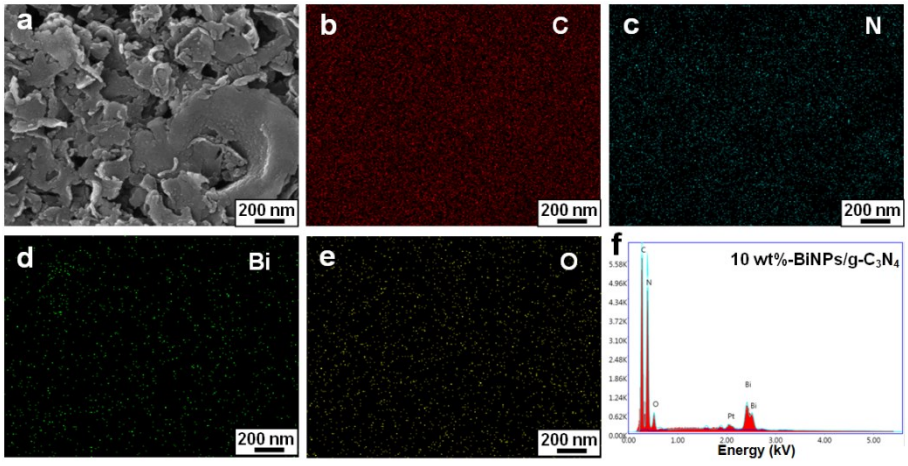


**Fig. S4.** EDS element mapping analysis of the 10 wt%-BiNPs/g-$C_3N_4$ nanocomposite.

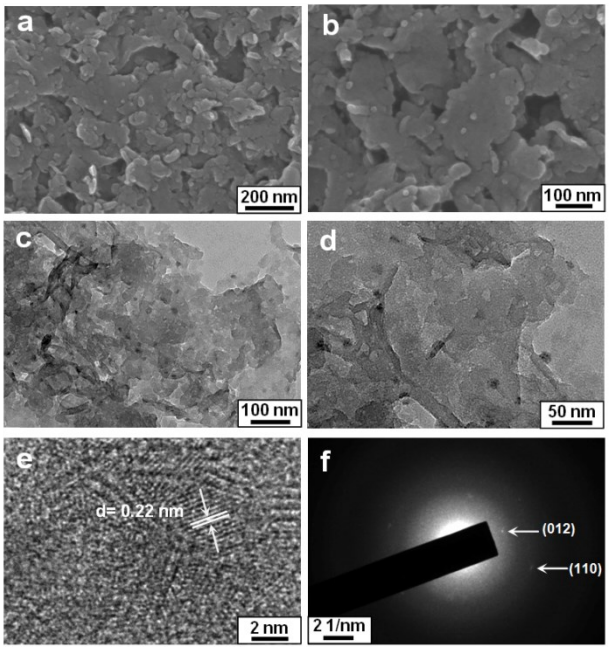


**Fig. S5.** Electron micrographs of the 2 wt%-BiNPs/g-$C_3N_4$ nanocomposite. (a,b) SEM micrographs of the sample, (c,d) TEM images of the sample, (e) HR-TEM of the surface of nanosheet, (f) SAED pattern of the sample.

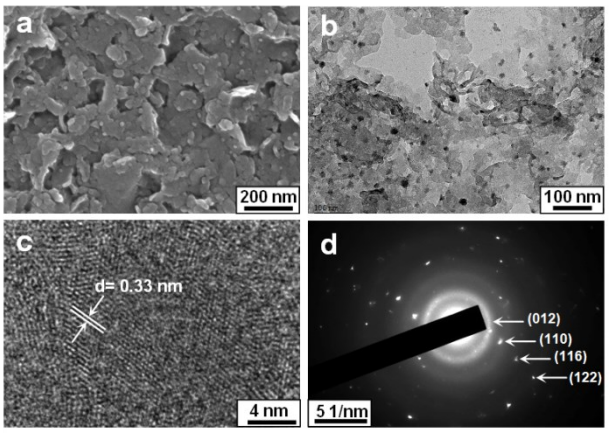


**Fig. S6.** Electron micrographs of the 4 wt%-BiNPs/g-$C_3N_4$ nanocomposite. (a) SEM and (b) TEM images of the sample, (c) HR-TEM micrograph of the surface of nanosheet, (d) the corresponding SAED pattern.

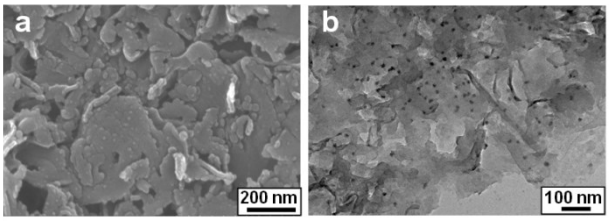


**Fig. S7.** Electron micrographs of the 8 wt%-BiNPs/g-$C_3N_4$ nanocomposite. (a) SEM and (b) TEM micrographs of the sample.

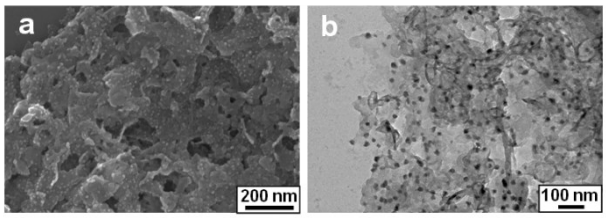


**Fig. S8.** Electron micrographs of the 12 wt%-BiNPs/g-$C_3N_4$ nanocomposite. (a) SEM and (b) TEM micrographs of the sample.

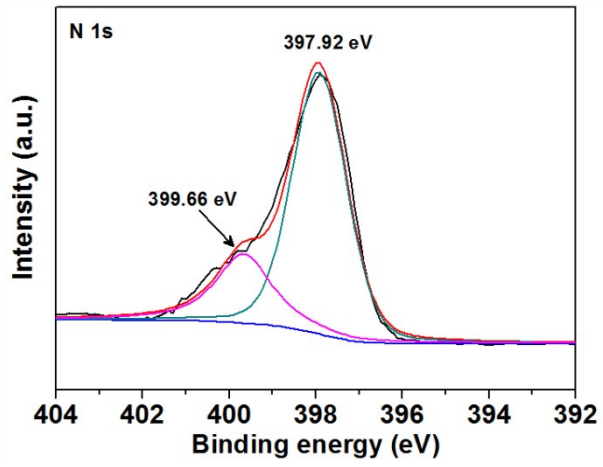


**Fig. S9.** XPS spectrum of N 1s region of the g-$C_3N_4$ nanosheet.

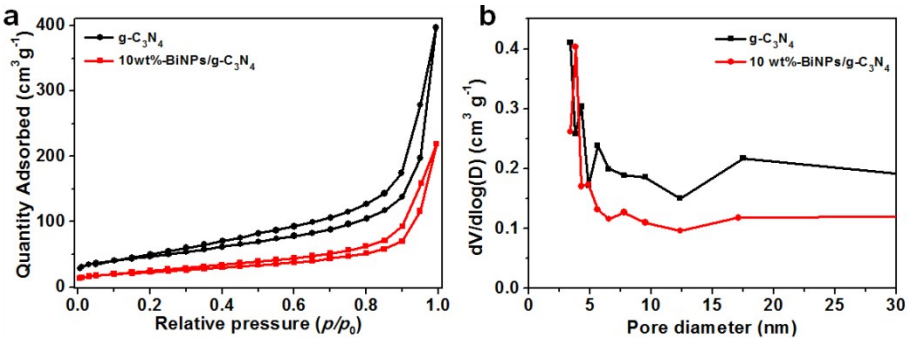


**Fig. S10.** (a) $N_2$ adsorption-desorption isotherm and (b) pore size distribution profile of the g-$C_3N_4$ nanosheets and 10 wt%-BiNPs/g-$C_3N_4$ nanocomposite.

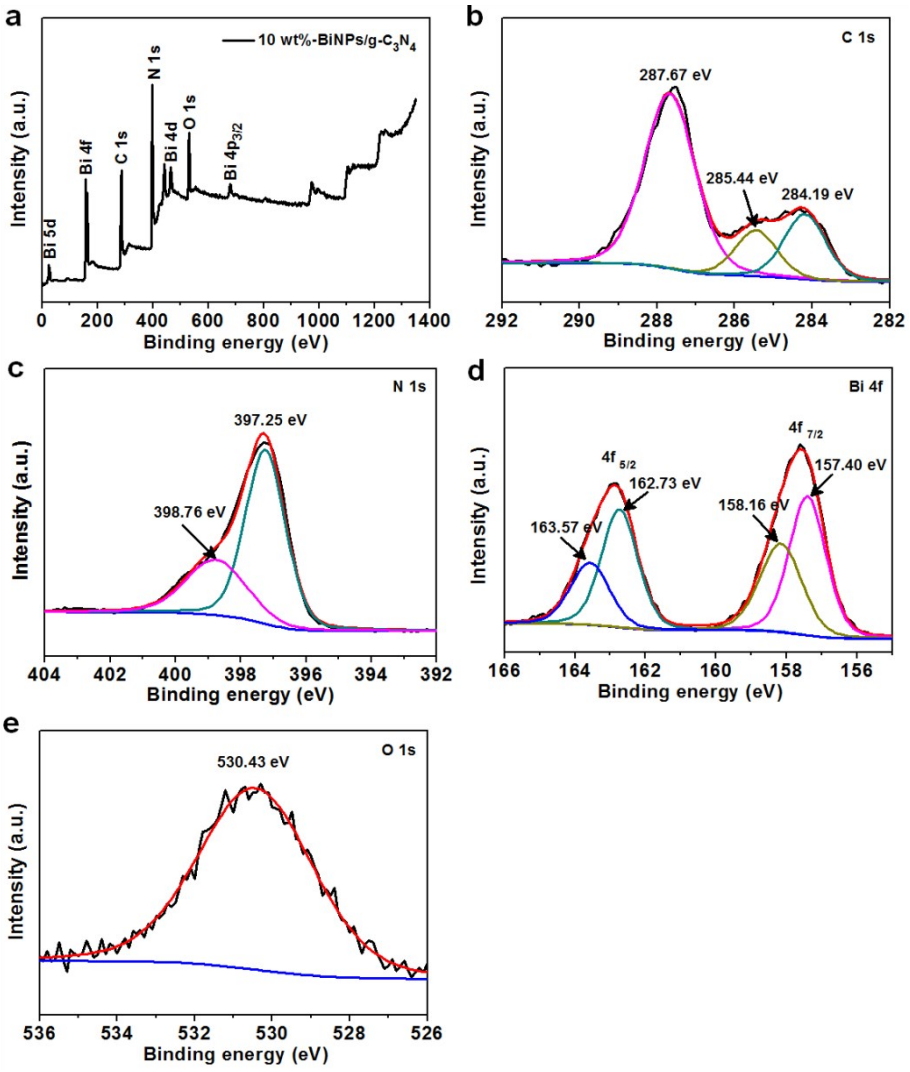


**Fig. S11.** (a) Survey XPS spectrum of the 10 wt%-BiNPs/g-$C_3N_4$ nanocomposite after photocatalytic degradation reaction. High-resolution XPS spectra of C 1s (b), N 1s (c), Bi 4f (d) and O 1 s (e) regions of the sample.

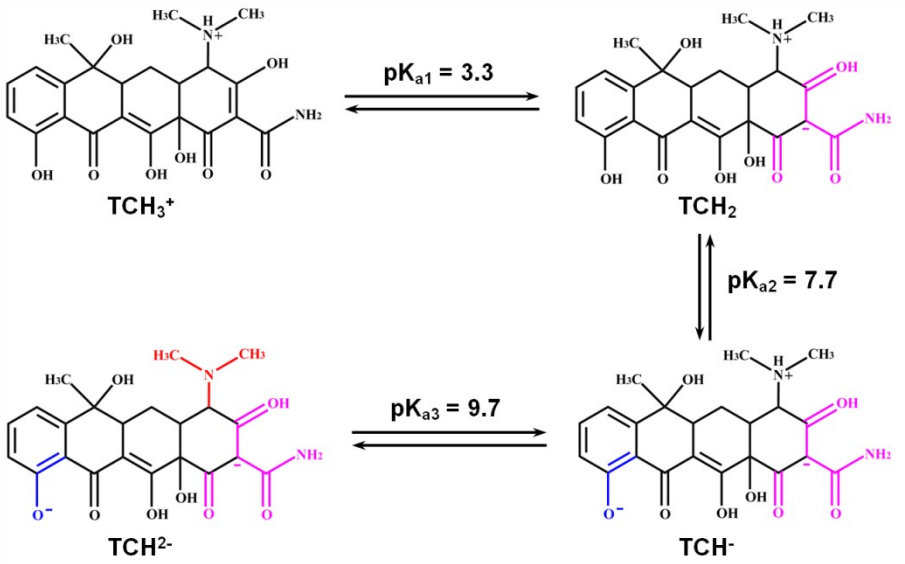


**Fig. S12.** pH dependant specification and molecular structure of TC-H under variable pH values.

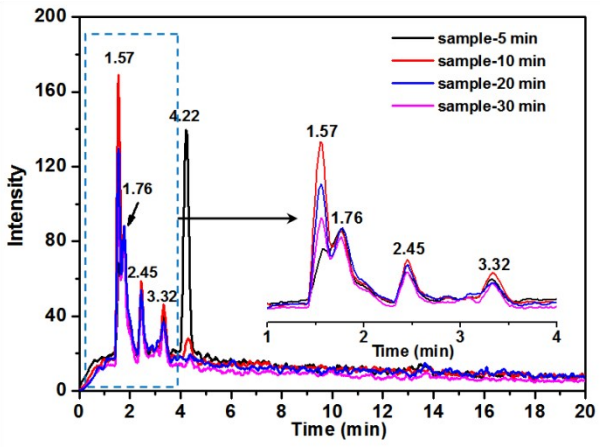


**Fig. S13.** The total ion chromatograms (TICs) of the photodegradation mixtures at different light irradiation time points.

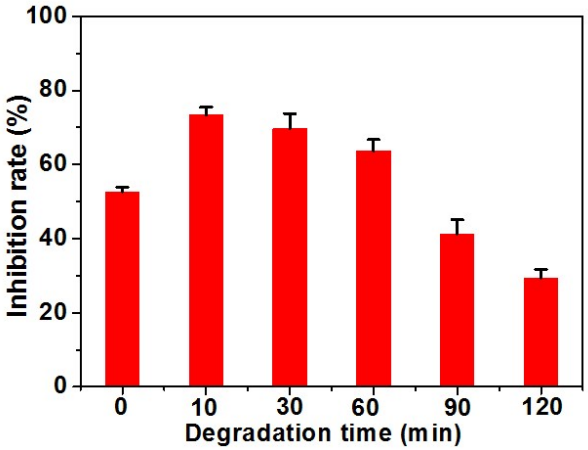


**Fig. S14.** Toxicity evaluation of the photodegradation mixtures by 10 wt% BiNPs/g-$C_3N_4$ at different minutes with the initial TC-H concentration of 20 mg $L^{-1}$.

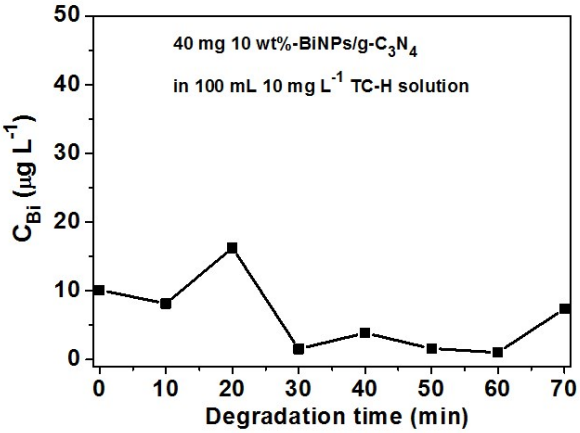


**Fig. S15.** Release of bismuth ions during the photocatalytic reaction process.

**Table. S1.** Kinetic parameters of the photoluminescence decays analysis of the g-$C_3N_4$ and 10 wt%-BiNPs/g-$C_3N_4$.

| Samples | Component | Life time (ns) | Relative percentage (%) | $\chi^2$ |
|---|---|---|---|---|
| g-$C_3N_4$ | $\tau_1$ | 2.3355 | 38.70 | 1.021 |
| | $\tau_2$ | 9.1681 | 61.30 | |
| 10 wt%-BiNPs/g-$C_3N_4$ | $\tau_1$ | 1.7998 | 43.63 | 1.217 |
| | $\tau_2$ | 7.5409 | 56.37 | |

**Table S2.** Comparison of photocatalytic activity of the BiNPs/g-$C_3N_4$ nanocomposite with various previously reported g-$C_3N_4$-based photocatalysts for degradation of TC-H.

| Catalysts | Mass of catalyst | TC-H reactant solution | Light source | Reduction efficiency | Ref. |
|---|---|---|---|---|---|
| BiNPs/g-$C_3N_4$ | 40 mg | 100 mL, 10 mg $L^{-1}$ | 300 W Xe lamp (λ>420 nm) | 70 min, 90.7 % | This work |
| AgNPs/g-$C_3N_4$ | 100 mg | 100 mL, 10 mg $L^{-1}$ | 300 W Xe lamp (λ>420 nm) | 120 min, 83 % | [1] |
| Urea-derived g-$C_3N_4$ | 40 mg | 100 mL, 10 mg $L^{-1}$ | 300 W Xe lamp (λ>420 nm) | 60 min, 79 % | [2] |
| h-BN/g-$C_3N_4$ | 100 mg | 100 mL, 10 mg $L^{-1}$ | 300 W Xe lamp (λ>420 nm) | 60 min, 79.7 % | [3] |
| CQDs/g-$C_3N_4$ | 50 mg | 100 mL, 10 mg $L^{-1}$ | 300 W Xe lamp (λ>420 nm) | 240 min, 78.6% | [4] |
| GQDs/mpg-$C_3N_4$ | 50 mg | 50 mL,20 mg $L^{-1}$ | 300 W Xe lamp (λ>400 nm) | 120 min, 65% | [5] |
| N-CNT/mpg-$C_3N_4$ | 50 mg | 50 mL, 20 mg $L^{-1}$ | 300 W Xe lamp (λ>420 nm) | 240 min, 67.1% | [6] |
| Mg/O co-decorated g-$C_3N_4$ | 100 mg | 100 mL, 30 mg $L^{-1}$ | 12 W LED lamp (>400 nm) | 120 min, 82% | [7] |
| Er-doped g-$C_3N_4$ | 25 mg | 50 mL, 25 mg $L^{-1}$ | 35 W xenon lamp | 90 min, 82% | [8] |
| Bi/$\alpha$-$Bi_2O_3$/g-$C_3N_4$ | 50 mg | 50 mL, 10 mg $L^{-1}$ | 300 W Xe lamp (λ>420 nm) | 180 min, 92% | [9] |
| $V_2O_5$/g-$C_3N_4$ | 50 mg | 100mL, 10 mg $L^{-1}$ | 250 W Xe lamp(λ>420 nm) | 120 min, 75.7% | [10] |
| CoP-HCCN | 40 mg | 100 mL, 10 mg $L^{-1}$ | 500 W Xe lamp (λ>420 nm) | 120 min, 96.7% | [11] |
| $Bi_2WO_6$/g-$C_3N_4$ | 50 mg | 50 mL, 10 mg $L^{-1}$ | 250 W Xe lamp (λ>420 nm) | 60 min, 73% | [12] |
| $WO_3$/g-$C_3N_4$/$Bi_2O_3$ | 100 mg | 100 mL, 10 mg $L^{-1}$ | 300 W Xe lamp (λ>420 nm) | 60 min, 80.2% | [13] |

CQDs: Carbon quantum dots; GQDs: Graphene quantum dots; CoP-HCCN: CoP co-catalyst modified high-crystalline g-$C_3N_4$ (HCCN).

## References


1. Z. Ren, F. Chen, K. Wen and J. Lu, Enhanced photocatalytic activity for tetracyclines degradation with Ag modified g-$C_3N_4$ composite under visible light, *J. Photoch. Photobio A*, 2020, **389**, 112217−112228.
2. C. Tian, H. Zhao, J. Mei and S. Yang, Cost-efficient graphitic carbon nitride as an effective photocatalyst for antibiotic degradation: An insight into the effects of different precursors and coexisting ions, and photocatalytic mechanism, *Chem. Asian J.*, 2019, **14**, 162−169.
3. L. Jiang, X. Yuan, G. Zeng, Z. Wu, J. Liang, X. Chen, L. Leng, H. Wang and H. Wang, Metal-free efficient photocatalyst for stable visible-light photocatalytic degradation of refractory pollutant, *Appl. Catal. B-Environ.* 2018, **221**, 715−725.
4. Y. Hong, Y. Meng, G. Zhang, B. Yin, Y. Zhao, W. Shi and C. Li, Facile fabrication of stable metal-free CQDs/g-$C_3N_4$ heterojunctions with efficiently enhanced visible-light photocatalytic activity, *Sep. Purif. Technol.*, 2016, **171**, 229−237.
5. J. Liu, H. Xu, Y. Xu, Y. Song, J. Lian, Y. Zhao, L. Wang, L. Huang, H. Ji and H. Li, Graphene quantum dots modified mesoporous graphite carbon nitride with significant enhancement of photocatalytic activity, *Appl. Catal. B-Environ.*, 2017, **207**, 429−437.
6. J. Liu, Y. Song, H. Xu, X. Zhu, J. Lian, Y. Xu, Y. Zhao, L. Huang, H. Ji and H. Li, Non-metal photocatalyst nitrogen-doped carbon nanotubes modified mpg-$C_3N_4$: Facile synthesis and the enhanced visible-light photocatalytic activity, *J. Colloid Interf. Sci.*, 2017, **494**, 38−46.
7. X. Wu, M. Fu, P. Lu, Q. Ren and C. Wang, Unique electronic structure of Mg/O co-decorated amorphous carbon nitride enhances the photocatalytic tetracycline hydrochloride degradation, *Chinese J.Catal.*, 2019, **40**, 776−785.
8. G. Li, B. Wang, J. Zhang, R. Wang and H. Liu, Er-doped g-$C_3N_4$ for photodegradation of tetracycline and tylosin: High photocatalytic activity and low leaching toxicity, *Chem. Eng. J.*, 2020, **391**, 123500−123505.
9. D. Chen, S. Wu, J. Fang, S. Lu, G. Zhou, W. Feng, F. Yang, Y. Chen and Z. Fang, A nanosheet-like $\alpha$-$Bi_2O_3$/g-$C_3N_4$ heterostructure modified by plasmonic metallic Bi

and oxygen vacancies with high photodegradation activity of organic pollutants, *Sep. Purif. Technol.*, 2018, **193**, 232−241.

10. Y. Hong, Y. Jiang, C. Li, W. Fan, X. Yan, M. Yan and W. Shi, In-situ synthesis of direct solid-state Z-scheme $V_2O_5$/g-$C_3N_4$ heterojunctions with enhanced visible light efficiency in photocatalytic degradation of pollutants, *Appl. Catal. B-Environ.*, 2016, **180**, 663−673.
11. F. Guo, X. Huang, Z. Chen, H. Sun and L. Chen, Prominent co-catalytic effect of CoP nanoparticles anchored on high-crystalline g-C3N4nanosheets for enhanced visible-light photocatalyticdegradation of tetracycline in wastewater, *Chem. Eng. J.*, 2020, **395**, 125118−125130.
12. H. Che, C. Liu, W. Hu, H. Hu, J. Li, J. Dou, W. Shi, C. Li and H. Dong, NGQD active sites as effective collectors of charge carriers for improving the photocatalytic performance of Z-scheme g-$C_3N_4$/$Bi_2WO_6$ heterojunctions, *Catal. Sci. Technol.*, 2018, **8**, 622−631.
13. L. Jiang, X. Yuan, G. Zeng, J. Liang, X. Chen, H. Yu, H. Wang, Z. Wu, J. Zhang and T. Xiong, *In-situ* synthesis of direct solid-state dual Z-scheme $WO_3$/g-$C_3N_4$/$Bi_2O_3$ photocatalyst for the degradation of refractory pollutant, *Appl. Catal. B-Environ.*, 2018, **227**, 376−385.